Analysis of the Electron Paramagnetic Resonance Spectrum of a Radical Intermediate in the Coenzyme B_{12}-Dependent Ethanolamine Ammonia-Lyase Catalyzed Reaction of *S*-2-Aminopropanol†

Vahe Bandarian‡ and George H. Reed*

Department of Biochemistry, University of Wisconsin-Madison, Madison, Wisconsin 53705

Received February 12, 2002; Revised Manuscript Received May 16, 2002

ABSTRACT: The structure of the steady-state radical intermediate in the deamination of *S*-2-aminopropanol catalyzed by ethanolamine ammonia-lyase (EAL) from *Salmonella typhimurium* has been probed by electron paramagnetic resonance (EPR) spectroscopy using isotopically labeled forms of the substrate and of the adenosylcobalamin cofactor. Electron spin−spin coupling between the radical, centered on the carbon skeleton of the substrate, and the low-spin Co^{2+} in cob(II)alamin (B_{12r}) produces a dominant splitting of the EPR signals of both the radical and the Co^{2+}. Analysis of the exchange and dipole−dipole contributions to the spin−spin coupling indicates that the two paramagnetic centers are separated by ∼11 Å. Experiments with ^{13}C- and with ^{2}H-labeled forms of *S*-2-aminopropanol show that the radical is centered on C1 of the carbon skeleton of the substrate in agreement with an earlier report [Babior, B. M., Moss, T. H., Orme-Johnson, W. H., and Beinert, H., (1974) *J. Biol. Chem. 249*, 4537−4544]. Experiments with perdeutero-*S*-2-aminopropanol and [2-^{15}N]-perdeutero-*S*-2-aminopropanol reveal a strong hyperfine splitting from the substrate nitrogen, which indicates that the radical is the initial substrate radical created by abstraction of a hydrogen atom from C1 of *S*-2-aminopropanol. The strong nitrogen hyperfine splitting further indicates that the amino substituent at C2 is approximately eclipsed with respect to the half-occupied *p* orbital at C1. Experiments with adenosylcobalamin enriched in ^{15}N in the dimethylbenzimidazole moiety show that the axial base of the cofactor remains attached to the Co^{2+} in a functional steady-state reaction intermediate.

Ethanolamine ammonia-lyase (EAL[1]; E. C. 4.3.1.7) is a bacterial enzyme that catalyzes a coenzyme B_{12}-dependent deamination of vicinal amino alcohols (*1*−*3*). Coenzyme B_{12}-dependent enzymes have been of interest for many years because their reaction mechanisms include highly reactive, radical intermediates (*4*−*10*). In all of these reactions, coenzyme B_{12} is believed to be a free radical initiator (*4*, *11*). Homolytic cleavage of the cobalt−carbon bond of the cofactor generates a pair of paramagnetic entities: a low-spin Co^{2+} secured within the corrin ring of the cofactor fragment (B_{12r}) and a highly reactive alkyl radical, the 5′-deoxyadenosyl radical. The latter species is believed to initiate radical chemistry by abstraction of a hydrogen atom from either the substrate or some part of the host enzyme. In the coenzyme B_{12}-dependent ribonucleotide reductase (*12*), in glutamate mutase (*13*), and in methylmalonyl CoA mutase (*14*), intermediates in which the organic radicals and the low-spin Co^{2+} of B_{12r} are strongly exchange coupled ($|J| > \sim 0.45$ cm^{-1}) in "biradical triplet states" have been characterized by EPR spectroscopy.

Earlier EPR studies of intermediates during the steady-state of the EAL reaction with a slow substrate, *S*-2-aminopropanol, revealed the presence of an interacting pair of paramagnetic species—an organic radical and low-spin Co^{2+} of B_{12r} (*15*). The EPR signal of the organic radical was split into an asymmetric doublet due to magnetic interactions with the unpaired electron in the d_{z2} orbital of Co^{2+} (*16*). EPR measurements with ^{2}H- and with ^{13}C-enriched forms of *S*-2-aminopropanol showed narrowing and broadening, respectively, consistent with the organic radical being localized at C1 of the carbon skeleton of the substrate (*15*). Subsequent measurements by electron spin−echo envelope modulation spectroscopy detected weak coupling of the radical to a ^{14}N nucleus that was not part of the substrate and did not originate from the amino group of the substrate (*17*, *18*).

Earlier analysis of the EPR spectra of the radical pair in EAL and in the related enzyme, dioldehydrase, suggested that splitting of the radical signal was due to an isotropic exchange interaction between the radical and the low-spin Co^{2+} of B_{12r} (*16*). Subsequently, more detailed analysis indicated that the magnetic coupling between the two paramagnetic centers included both isotropic exchange and

† This research was supported by NIH Grant GM35752.

* Address correspondence to George H. Reed, University of Wisconsin, 1710 University Avenue, Madison, WI 53705, Email: reed@biochem.wisc.edu.

‡ Present address: Univ. of Michigan, Biophys. Res. Div., Chem. Sci. Bldg., 930 N University, Ann Arbor, MI 48109-1055.

[1] Abbreviations: EAL, ethanolamine ammonia-lyase; coenzyme B_{12}, adenosylcobalamin; B_{12r}, cob(II)alamin; EPR, electron paramagnetic resonance; CW, continuous wave; NMR, nuclear magnetic resonance; ENDOR, electron nuclear double resonance; zfs, zero-field splitting; Hepes, *N*-2-hydroxyethylpiperazine-*N*′-2-ethane-sulfonic acid; ^{15}N-enriched coenzyme, [42% ^{15}N-dimethylbenzimidazole, 58%^{14}N-dimethylbenzimidazole] coenzyme B_{12}.

10.1021/bi0201217 CCC: $22.00
Published on Web 06/18/2002

through-space, dipole−dipole interactions (*19*). Both of these magnetic interactions depend on the spatial separation of the paramagnets in the radical pair. Potential complications arising from *g*-anisotropy of the low-spin Co^{2+}, including anisotropies in the exchange interaction, have also been discussed (*20*). Recent experiments have suggested that a product radical may be the species observed in the steady-state with ethanolamine as the substrate (*21*).

The availability of a recombinant form of EAL from *Salmonella typhimurium* (*22*, *23*) together with convenient methods for resolution enhancement in EPR signals (*24*) prompted more detailed studies of the characteristics of the CW EPR spectra of the radical intermediate in the reaction of EAL with *S*-2-aminopropanol. Resolution enhancement of the radical doublet component in the EPR spectrum of the steady-state intermediate in the reaction with *S*-2-aminopropanol reveals hyperfine splitting from nuclear spins within the substrate fragment. The resolution enhanced spectra also provide improved targets for analysis of the electron−electron spin−spin interactions that dominate the spectra. The present paper reports results of this analysis.

EXPERIMENTAL PROCEDURES

Materials. Recombinant *S. typhimurium* EAL was overexpressed in *Escherichia coli* and purified as described previously (*25*). The specific activity of the enzyme was 54 IU (mg of protein)$^{-1}$ with ethanolamine as substrate. Coenzyme B_{12} was purchased from Sigma. Coenzyme B_{12} enriched to 50% in ^{15}N in the dimethylbenzimidazole moiety was a generous gift of Dr. Janos Rétey.

Synthesis of Isotopically Labeled Forms of 2-Aminopropanol. Labeled forms of *S*-2-aminopropanol were prepared essentially as described previously (*15*). The appropriately labeled L-alanine precursors (Cambridge Isotope Labs or Isotec) were converted to the respective methyl or ethyl esters and reduced with $LiAlH_4$ or $LiAlD_4$. The precursors for the synthesis of [1-^{13}C,1,1,2,3,3,3-$^2H_6$]-*S*-2-aminopropanol and [2-^{15}N,1,1,2,3,3,3-$^2H_6$]-*S*-2-aminopropanol were [1-^{13}C,2,3,3,3-$^2H_4$]-L-alanine and [2-^{15}N, 2,3,3,3-$^2H_4$]-L-alanine, respectively. These labeled compounds were prepared from the corresponding protio forms using glutamic pyruvic transaminase, which catalyzes exchange the protons at 2 and 3 positions of L-alanine with deuterons from ^2H_2O, using the reaction conditions previously described (*26*). The exchange reaction was monitored by ^1H NMR. Deuterium incorporation at carbons 2 and 3 of the L-alanine was 95% complete within 20 h. At the end of the incubation, the enzyme was removed using Millipore concentrators (10 000 cutoff). The filtrate was acidified and applied to a column of Dowex 50 × 8 (H^+ form). The column was washed with water, and the L-alanine was eluted with a 0−1 M gradient of HCl. Fractions containing the L-alanine were collected and lyophilized.

EPR Measurements. EPR spectra were recorded at X-band with a Varian E-3 EPR spectrometer and a standard liquid N_2 immersion Dewar. The spectrometer was interfaced to a microcomputer for data acquisition. Resolution enhancement was performed as described previously (*24*). Samples for EPR measurements were obtained by mixing EAL (~0.2 mM active sites−six site/oligomer), 0.4 mM coenzyme B_{12}, 25 mM *S*-2-aminopropanol, and 10 mM Hepes/NaOH, pH 7.5, in a total volume of 0.25 mL. The solution was transferred to an EPR tube and frozen within 20 s of mixing. For the samples prepared in ^2H_2O, EAL was exchanged into ^2H_2O by lyophilization and resuspension in ^2H_2O. The samples of enzyme were then mixed with ^2H_2O solutions of substrate and coenzyme B_{12}.

Rapid-Mix Freeze-Quench EPR. An Update Instruments (Madison, WI) model 745 RAM rapid-mix freeze quench apparatus was used to prepare samples for EPR measurements. The experiments were performed in a two syringe setup where one syringe was filled with a mixture of EAL (0.21 mM), coenzyme B_{12} (1.2 mM), and Hepes/NaOH pH 7.5 (10 mM), and the second syringe contained *S*-2-aminopropanol (10 mM) and Hepes/NaOH pH 7.5 (10 mM). The two solutions were mixed, pushed through aging hoses of various lengths, and injected into funnels containing isopentane maintained at ~ −140 °C. The resulting snow was packed into quartz EPR tubes that had been attached to the end of the funnel. The EPR spectra were obtained at 77 K.

Spectral Simulations. EPR spectra of intermediates in EAL are dominated by spin−spin interactions between the unpaired electron from an organic radical and the odd electron from the proximate, low-spin Co^{2+} in B_{12r} (*16*, *19*, *27*). The complex EPR patterns are most readily interpreted with the aid of the following spin Hamiltonian:

$$\mathscr{H}_s = \beta \vec{H}\cdot\mathbf{g_1}\cdot\vec{S}_1 + \beta \vec{H}\cdot\mathbf{g_2}\cdot\vec{S}_2 + J\vec{S}_1\vec{S}_2 + \vec{S}_1\cdot\mathbf{D}\cdot\vec{S}_2 + \mathscr{H}_{HF} \quad (1)$$

where the first two terms represent the Zeeman interaction of the low-spin Co^{2+} and radical, respectively; the third term is the isotropic exchange interaction; the fourth term is the electron spin dipole−dipole coupling; and $\mathscr{H}_{HF}$ represents the nuclear hyperfine interactions present at each center:

$$\mathscr{H}_{HF} = \sum_{j=1}^{n} K_j(\theta,\phi)\hat{I}_{jz}\hat{S}_{1z} + \sum_{k=1}^{m} K_k(\theta,\phi)\hat{I}_{kz}\hat{S}_{2z}. \quad (2)$$

In eq 2, $K_j(\theta,\phi)$ and $K_k(\theta,\phi)$ are the first-order expressions for hyperfine interactions (*28*). The smaller nuclear Zeeman and nuclear quadrupolar interaction terms were not included in the analysis. The tensors in eq 1 are diagonal in their individual principal axis systems which are not necessarily collinear with those of other terms. The *g*-axis system of Co^{2+} was used as the reference axis in the molecular frame. Previous studies with suicide inactivators, hydroxyethylhydrazine (*25*) and glycolaldehyde (*29*), indicated that radicals produced from these analogues were positioned approximately along the *z*-axis of Co^{2+} (i.e., perpendicular to the corrin ring). Hence, the starting assumption was that the Co^{2+} to radical interspin vector was along the *z*-axis of Co^{2+}. Wigner rotation matrices are used to transform the dipole−dipole interaction, expressed as a conventional zfs tensor, into the laboratory frame of reference (*25*, *30*). The same Euler angles were used to express the *g* and hyperfine tensors in the laboratory frame. Procedures for diagonalization of the energy matrix and simulation of field-swept powder EPR spectra were described previously (*25*). Potential complications in the spectra from the *g*-anisotropy of the Co^{2+} and from a possible off-axis alignment of the interspin vector are discussed in the appendix.

Combined Effects of J and D on EPR Powder Patterns. The separate identities of the radical and low spin Co^{2+} signals in the EPR spectra indicate that the electron spin−spin coupling in this ensemble is in the "weak exchange" regime (*27*). In the weak exchange situation, the isotropic exchange interaction, *J*, produces a doublet splitting of the EPR signals of each partner (*16*). The dipole−dipole interaction, *D*, gives rise to a "Pake pattern" for each spin (*31*). The combined effects of *J* and *D*, in the regime where the interactions are comparable in magnitude, is a Pake pattern wherein the magnitudes of the splittings at the turning points are altered by *J* (*25*). In the Pake pattern, turning points indicative of the magnetic field along the interspin vector ($\theta = 0°$), are split by 2*D*, whereas orthogonal to the interspin vector ($\theta = 90°$), the splitting is *D*. Inclusion of the exchange interaction alters this splitting such that at $\theta = 0°$ and $\theta = 90°$ the splittings are $|J + 2D|$ and $|J - D|$, respectively. For the sign convention adopted in eq 1, an antiferromagnetic exchange interaction corresponds to a positive *J*. The dipole−dipole interaction parameter, *D*, is negative (*32*). Thus, for antiferromagnetic exchange coupling, the two terms combine constructively at $\theta = 90°$ and destructively at $\theta = 0°$; the opposite situation prevails for ferromagnetic exchange. The powder patterns are therefore sensitive to the relative signs of *J* and *D*. Transition probabilities (obtained from the matrix of eigenvectors) of the halves of the doublet are influenced by the magnitude of *J* relative to the difference in the *g* values of the radical and low-spin Co^{2+}.

The *g*-anisotropy of the low-spin Co^{2+} alone produces a resolved powder pattern for Co^{2+} transitions having turning points with the magnetic field parallel ($g_{||} = 2.01$) to the d_{z2} orbital and perpendicular ($g_{\perp} = 2.26$) to this orbital (*27*, *33*). The $g_{||}$ signals of Co^{2+} are split by $|J + 2D|$ and the $g_{\perp}$ signals by $|J - D|$. If the interspin vector is not aligned along a principal axis of Co^{2+}, a rhombic, or E term, is present, which could create an additional splitting of the signals both of the Co^{2+} and of the radical whenever magnetic field is in the *xy* plane of the *g*-axis system of Co^{2+}. Calculations in the appendix, however, indicate that the assumption of an axially symmetric dipole−dipole interaction ($E = 0$), independent of the alignment of the interspin vector, is valid for the modest *g*-anisotropy of the low-spin Co^{2+} and X-band microwave frequencies. The *g*-anisotropy of the low-spin Co^{2+} does, however, result in a small "pseudo isotropic" contribution from the dipole−dipole interaction that appears as a contribution to *J* (*34*).

RESULTS AND DISCUSSION

EPR Spectrum of the Intermediate with S-2-Aminopropanol. Samples of EAL frozen within 30 s of mixing with coenzyme B_{12} and *S*-2-aminopropanol exhibit (Figure 1) the characteristic EPR spectrum described previously (*15*, *35*). The spectrum may be divided into signals from the low-spin Co^{2+} centered at $g_{\perp} = 2.26$ and $g_{||} = 2.01$ and a prominent, asymmetric doublet centered at $g = 2.00$ assigned to the radical. ^{59}Co ($I = 7/2$) hyperfine splitting is present in the $g_{||}$ region ($A_{||} \sim 100$ G). The ^{59}Co hyperfine splitting is unresolved in the $g_{\perp}$ region ($A_{\perp} < 10$ G) (*27*). The inset of Figure 1 shows some of the ^{59}Co hyperfine transitions in the $g_{||}$ region. The doublet splitting of the organic radical and the altered appearance of the signals from B_{12r} are due to the electron spin−spin interaction between the two paramagnetic centers (*16*).

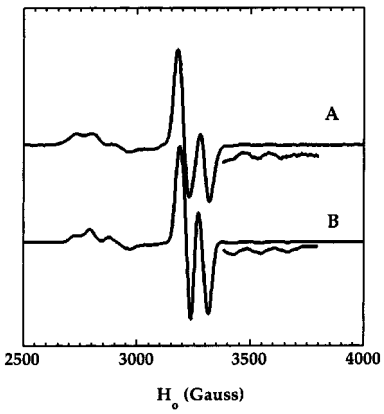

FIGURE 1: Radical doublet EPR spectrum with *S*-2-aminopropanol. The experimental EPR spectrum (A) was obtained by mixing EAL (~0.2 mM active sites), 0.4 mM coenzyme B_{12}, 25 mM *S*-2-aminopropanol, and 10 mM Hepes/NaOH, pH 7.5 in a total volume of 0.25 mL. The solution was transferred to an EPR tube and frozen within 20 s of mixing. The EPR spectrum (A) was obtained at 77 K. A representative simulation of the spectral envelope is shown in (B**)**. The exchange (*J*) and dipole−dipole interactions (*D*) were set to 70 and −23 G, respectively. The components of the radical and the Co^{2+} *g*-tensors were $g_{xx} = 2.0043$, $g_{yy} = 2.0037$, $g_{zz} = 2.0021$ and $g_{xx} = 2.26$, $g_{yy} = 2.26$ and $g_{zz} = 2.01$, respectively. The hyperfine interaction of the unpaired electron on the cobalt with the Co^{2+} nuclear spin ($I = 7/2$), and the superhyperfine splitting from the ^{14}N ($I = 1$) of the dimethylbenzimidazole lower axial ligand were set to $A_{xx} = A_{yy} = 10$ G, $A_{zz} = 120$ G and $A_N = 20$ G, resectively. A Lorentzian line shape was used with an axial line width of $l_{xx} = l_{yy} = 20$ G, $l_{zz} = 15$ G for Co^{2+} and an isotropic line width of 20 G for the organic radical. The powder patterns were obtained by numerical integration of an axially symmetric powder pattern (*57*). The insets for each plot represent a vertical expansion of the corresponding region of spectrum.

Time Course for Appearance of the EPR Spectrum. To confirm that the complex EPR spectrum (Figure 1) arises from a species that can be an authentic intermediate in the normal reaction sequence, the time course of the appearance of the EPR spectrum was determined by rapid-mix freeze-quench methods. A solution containing EAL and coenzyme B_{12} was mixed with a solution containing substrate, and the mixture was aged various times prior to freezing. The time course for appearance of the EPR spectrum is shown in Figure 2. Under these conditions, the radical doublet formed at a rate of 140 s^{-1}. The rate of appearance of the EPR signals is greater than the k_{cat} (~0.3 s^{-1}) measured for *S*-2-aminopropanol. Therefore, the steady-state intermediate detected by EPR appears at a rate that is more than sufficient to satisfy the requirements of kinetic competence.

The Electron Spin−Spin Interactions. One anticipates that the spectral envelope of signals originating from the radical intermediate encompasses hyperfine splitting from nuclear spins of the radical as well as fine structure from the exchange and dipole−dipole interaction with the nearby low-spin Co^{2+}. Elimination of ^1H hyperfine splitting from carbon-bound and solvent exchangeable (hydroxyl and amino) positions, through deuteration, simplifies analysis of the underlying electron spin−spin interaction. Hence, the EPR spectrum obtained with [1,1,2,3,3,3-$^2H_6$]-*S*-2-aminopropanol in ^2H_2O solution was the initial object of the analysis (Figure 3A). Under these conditions, the only residual source of strong nuclear hyperfine splitting in the radical signal is the

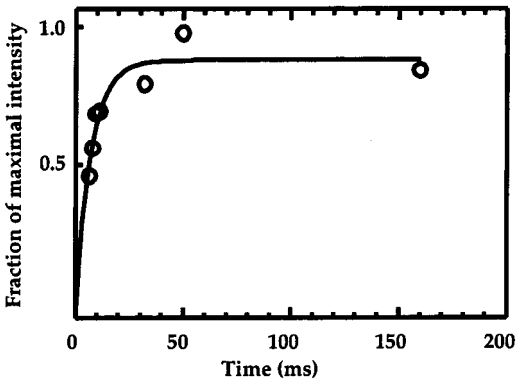

FIGURE 2: Kinetic competence of the radical doublet EPR signal. In these experiments, a solution of EAL and coenzyme B12 was mixed with a solution of *S*-2-aminopropanol, and the rate of formation of the radical doublet signal was monitored as function of time. Comparisons of the double integrals of signals of the radical with those of a sample of Varian strong pitch indicate that at 160 ms the radical signal corresponds to ~3 radical spins per enzyme oligomer.

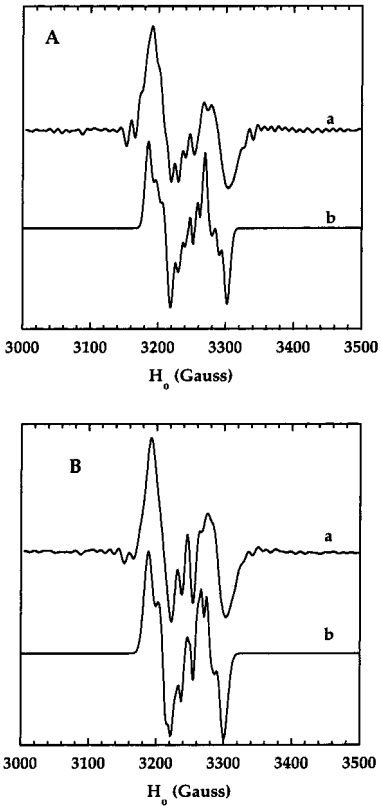

FIGURE 3: Comparison of resolution enhanced experimental (a) and simulated (b) EPR spectra obtained with [1,1,2,3,3,3-$^2H_6$]-*S*-2-aminopropanol (A) and with [1,1,2,3,3,3-$^2H_6$, 2-^{15}N]-*S*-2-aminopropanol (B) in ^2H_2O and coenzyme B_{12}. The samples were prepared and EPR spectra were obtained as described in the legend for Figure 1. The simulations were obtained using the parameters described for the simulation in Figure 1. The interaction between the unpaired electron of the organic radical and the ^{14}N (Figure 3A) or ^{15}N (Figure 3B) of the substrate was set to 11 and 15.4 G, respectively. Orientation dependent Lorentzian line shapes were used to reproduce the spectral envelopes for the simulation in Figure 3Ab ($l_{xx} = l_{yy} = 6$ G, $l_{zz} = 2.5$ G) and Figure 3Bb ($l_{xx} = l_{yy} = 8$ G, $l_{zz} = 2.5$ G). Transitions due to Co^{2+} were suppressed in the simulations.

^{14}N ($I = 1$) of the amino group. Indeed, a ^{14}N triplet splitting is present in the resolution enhanced spectrum of the radical

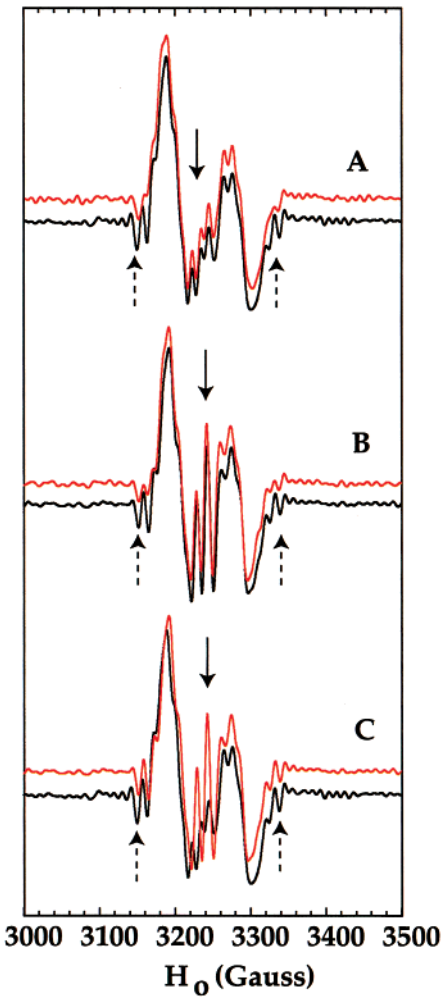

FIGURE 4: EPR spectra obtained for samples of EAL mixed with [1,1,2,3,3,3-$^2H_6$]-*S*-2-aminopropanol or with [1,1,2,3,3,3-$^2H_6$, 2-$^{15}N_1$]-*S*-2-aminopropanol and with unlabeled or ^{15}N-enriched coenzyme B_{12} in ^2H_2O. Panel A compares the spectra obtained with [1,1,2,3,3,3-$^2H_6$]- *S*-2-aminopropanol with unlabeled (black) or ^{15}N-enriched coenzyme B_{12} (red). Panel B shows the spectra obtained with [1,1,2,3,3,3-$^2H_6$, 2-$^{15}N_1$]-*S*-2-aminopropanol and either unlabeled (black) or ^{15}N-enriched coenzyme B_{12} (red). Panel C shows the overlay of spectra obtained with [1,1,2,3,3,3-$^2H_6$]-*S*-2-aminopropanol (black) and with [1,1,2,3,3,3-$^2H_6$, 2-$^{15}N_1$]-*S*-2-aminopropanol (red). The solid arrows show the positions in the spectra where nitrogen hyperfine splitting from the *S*-2-aminopropanol is conspicuous. The dashed arrows show positions in the spectra show where the nitrogen superhyperfine splittings from the dimethylbenzimidazole ligand to Co^{2+} are located in the ^{59}Co hyperfine transitions of the $g_{||}$ region of the Co^{2+} spectrum. The samples were prepared as described in the legend for Figure 1.

(Figure 3A). The triplet structure in the center of the spectrum changes to a doublet in analogous sample with [1,1,2,3,3,3-D_6, 2-^{15}N]-*S*-2-aminopropanol (Figure 3B).

There is, however, some hyperfine structure at the low and high field edges of the radical doublet signal that does not change upon substitution of ^{15}N into the substrate. Manipulation of the resolution enhancement parameters shows that these features are not "side lobes" due to the truncation of the time domain signal (*36*). Spectra obtained from samples made up from the ^{15}N-enriched coenzyme establish that these "edge" features are due to the nitrogen superhyperfine splitting of $g_{||}$ ^{59}Co hyperfine transitions which overlap with the signals of the radical (Figure 4). The measured ^{14}N superhyperfine splitting ($A_{14N} \sim 15$ G) from

the dimethylbenzimidazole axial ligand is smaller than in samples of EAL and B_{12r} ($A_{14N} \sim 19$ G) (*33*), a result consistent with the presence of an exchange interaction (*27*).

The overall appearance of the "radical doublet" spectrum (Figure 1) indicates that exchange interaction is larger than the dipole−dipole interaction and that the exchange interaction is antiferromagnetic, i.e., the interactions combine constructively whenever the magnetic field is perpendicular to the interspin vector. The opposite signs of J and D turn the Pake pattern "inwards" such that, in the radical transitions, signals corresponding to parts of the sample having orientations of the magnetic field along the interspin vector lie between the two major peaks of the doublet. The fact that the $g_{||}$ transitions of Co^{2+} are not split to the extent of those of the radical, in the perpendicular direction, further indicates that the exchange and dipole−dipole interactions counteract each other along the direction of $g_{||}$, i.e., the interspin vector appears to lie approximately along the z-axis of the Co^{2+} reference frame. The maximum splitting in the xy plane $|J - D|$ of the radical is ∼93 G, and the splitting along z is ∼ 24 G. The magnitudes of the splittings indicate that D is $\sim -23 \pm 5$ G, and $J \sim 70 \pm 5$ G. Simulations of the radical portion of the spectrum within this range of parameters provide an reasonable reproduction of the experimentally observed patterns (see Figures 1B, 3Ab, and 3Bb).

The distance between Co^{2+} and the radical is estimated from the expression in eq 3 (*37*):

$$R\,(\text{Å}) = \sqrt[3]{\frac{6.96 \times 10^3 \mathbf{g_1 g_2}}{D(G)}} \qquad (3)$$

The range of values for D indicates that R is between 10.2 and 11.9 Å. The ethanesemidione radical and hydrazine cation radical in EAL lie at about the same distance from Co^{2+} as the *S*-2-aminopropanol radical. However, the exchange interaction is significantly smaller for the former radicals (*25*, *29*). The larger exchange interaction in the substrate radical suggests that there is an effective pathway for superexchange with the Co^{2+}/*S*-2-aminopropanol-1-yl radical pair that is not present in the complexes with the unnatural radicals.

The range of values for the exchange coupling, J, obtained in the present analysis is close to values obtained in previous simulations wherein only the envelope of the radical doublet was reproduced (*16*). Previous simulations of the radical doublet using expressions from perturbation theory provided a range for R that is close to the values from the present analysis (*19*).

Nitrogen Hyperfine Interaction. Hyperfine splitting from the amino nitrogen ($a_{iso}^{14N} \sim 12$ G isotropic) determined from the analysis of the previous section is within the range (10−14 G) reported for similar radicals in solution (*38*, *39*). This relatively large splitting from ^{14}N is expected for a β-amino nitrogen that is nearly eclipsed with respect to the half occupied p orbital as illustrated in Scheme 1.

The assignment of the nitrogen splitting constant was confirmed by analysis of the spectrum obtained with [2-^{15}N,1,1,2,3,3,3-$^2H_6$]-*S*-2-aminopropanol (see Figure 3B).

α-*Proton Hyperfine Interaction.* The electron spin−spin parameters can be used to simulate the EPR spectra obtained

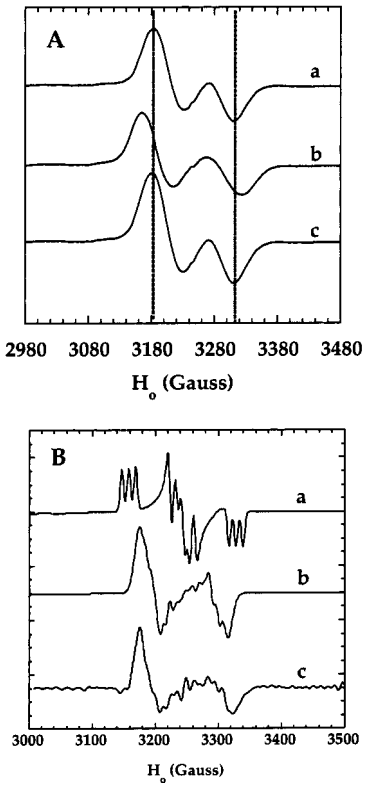

FIGURE 5: (A) Radical doublet region of the EPR spectra obtained with unlabeled (a) [1-^{13}C,1,1,2,3,3,3-$^2H_6$]-*S*-2-aminopropanol (b) and [2-^{13}C,1,1,2,3,3,3-$^2H_6$]-*S*-2-aminopropanol (c) in ^2H_2O. The samples were prepared and EPR spectra were obtained as described in the legend for Figure 1. (B) Simulation of the orientation dependence of the radical doublet region of the EPR spectrum obtained with [1-^{13}C,1,1,2,3,3,3-$^2H_6$]-*S*-2-aminopropanol and coenzyme B_{12} in ^2H_2O. The spin−spin parameters and the g-tensors were as described in the legend for Figure 1. The hyperfine coupling between the organic radical and the amino group nitrogen (^{14}N, $I = 1$) was set to 11 G. The g-tensor of the $^{59}Co^{2+}$ was chosen as the reference for rotations of the ^{13}C hyperfine tensor ($I = 1/2$, $A_{xx} = 8.6$ G, $A_{yy} = 8.6$ G, $A_{zz} = 76$ G). The simulation in (a) was obtained by rotating the ^{13}C hyperfine tensor to interchange the z component of the splitting, with perpendicular (xy) component. In (b), the z-component of the axial ^{13}C tensor was assumed to be collinear with the z-component of the g-tensor for B_{12r}. In each simulation, the principal components of a direction dependent line width function ($l_{xx} = 10$ G, $l_{yy} = 10$ G, $l_{zz} = 3$ G) were also rotated to overlap the ^{13}C tensor rotations. The experimental spectrum (c) is a resolution enhanced version of the spectrum shown in Figure 5A,b. Transitions due to Co^{2+} were suppressed in the simulations.

with [2,3,3,3-D_4]-*S*-2-aminopropanol in ^2H_2O (data not shown). The Euler angles and hyperfine splitting tensor are still being refined. The current best fit for the isotropic component of the splitting from the α-proton, (∼17 G), is in the same range observed in solution (17−20 G) (*38*, *39*).

EPR Spectra with ^{13}C-Labeled S-2-Aminopropanol. Figure 5A shows the EPR spectra obtained with unlabeled, [1-^{13}C]-*S*-2-aminopropanol, and [2-^{13}C]-*S*- 2-aminopropanol. The spectra confirm earlier observations and conclusions that significant spin density is localized to C-1 of *S*-2-aminopropanol (*15*). To simplify the simulations, EPR spectra were obtained from samples with [1-^{13}C;1,1,2,3,3,3-$^2H_6$]-*S*-2-aminopropanol and coenzyme B_{12} in ^2H_2O (Figure 5Bc). The EPR spectrum obtained from this sample was reproduced in simulations (Figure 5Bb) using the same set of parameters for the electron spin−spin interaction and nitrogen hyperfine interaction determined earlier and incorporation of an axial

Scheme 1

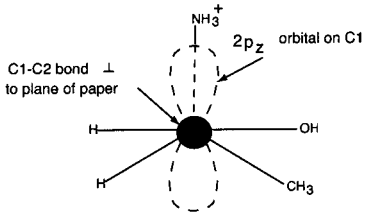

^{13}C hyperfine splitting tensor. Euler rotations of the ^{13}C tensor were not required, a result that indicates that the axis of the half occupied *p* orbital of the radical is approximately parallel to the *z*-axis of Co^{2+}.

Other Sources of Hyperfine Splitting. The radical signals of EPR spectra from samples prepared in ^2H_2O were narrowed with respect to those for samples prepared in H_2O (data not shown), and this observation is consistent with substantial hyperfine splitting from protons on the amino nitrogen and hydroxyl moieties of the substrate radical. Contributions from these four solvent-exchangeable protons could not be studied in isolation, and this source of hyperfine splitting was therefore eliminated from further study.

EPR spectra of samples in which the β-proton of *S*-2-aminopropanol was present (data not shown) indicated that β-proton hyperfine splittings were contributing to CW spectra. These small hyperfine splittings, however, are well suited for analysis by pulsed ENDOR spectroscopy of the corresponding samples ([2-^{2}H]-*S*-2-aminopropanol) with deuterium in place of the β-hydrogen. The resulting hyperfine coupling tensor of the β-deuteron ($A_\perp = 2.3$ MHz and $A_{||} = 3.6$ MHz) (obtained from ENDOR spectra) is consistent with the eclipsed conformation shown above (R. L. LoBrutto, V. Bandarian, and G. H. Reed, unpublished observations).

Active Site of EAL During Turnover. A working model for the active site of EAL during turnover with *S*-2-aminopropanol is shown in Figure 6. The *S*-2-aminopropanol radical is separated from the Co^{2+} of B_{12r} by ~11 Å and is aligned along the *z*-axis of the *g* reference frame of Co^{2+}. The half occupied *p* orbital of the radical lies parallel to the *z* axis of Co^{2+} as indicated by the Euler angles $\alpha = \beta = \gamma = 0$ of the C-1 ^{13}C hyperfine tensor in the reference frame of the Co^{2+}. Analysis of the electron spin−spin interactions also indicates that the Co^{2+} to radical interspin vector lies approximately along the *z*-axis of the Co^{2+} frame of reference. The observations of ^{14}N/^{15}N superhyperfine splitting (from the dimethylbenzimidazole ligand) in the ^{59}Co hyperfine transitions in the $g_{||}$ direction indicate that, in EAL, the coenzyme binds in a base-on mode in a functional intermediate state. This base-on binding mode was detected for isolated B_{12r} bound to EAL by CW EPR (*33*) and for B_{12r} in the intermediate state by electron spin−echo envelope modulation spectroscopy (*40*).

Mechanistic Implications. The ~11 Å separation between the radical and the Co^{2+} of B_{12r}, indicates that the B_{12r} does not play a direct role in the substrate rearrangement, e.g., by combining with the radical form of the substrate to form an organo-cobalt intermediate. A hypothetical model of the catalytic cycle of the reaction with *S*-2-aminopropanol is shown in Scheme 2. The present experiments show that the substrate radical accumulates in the steady state of the reaction, which suggests that the rearrangement step (reaction 3) is substantially rate determinining. This suggestion is

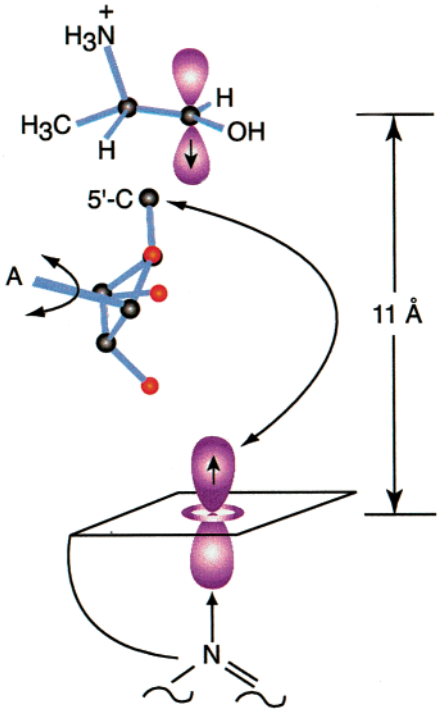

FIGURE 6: Schematic representation of the positions of the substrate radical, 5′-deoxyadenosine, and B_{12r} in the active site of EAL during turnover with *S*-2-aminopropanol. The Bzm represents the dimethylbenzimidazole which remains coordinated to the cobalt ion. The position of 5′-deoxyadenosine was obtained from ^{13}C ENDOR results (*46*).

Scheme 2

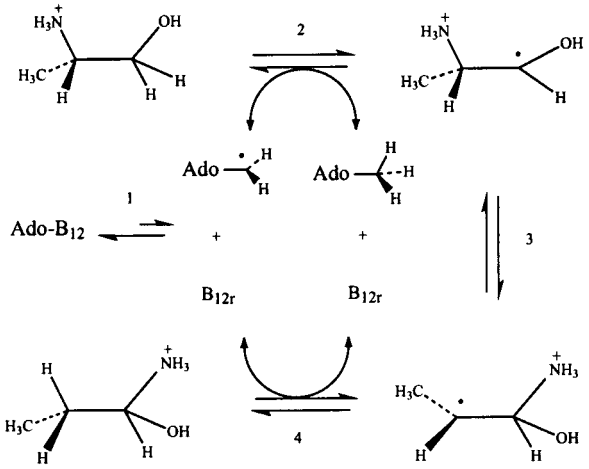

compatible with earlier observations of ^{3}H exchange from [5′-^{3}H] coenzyme B_{12} into *S*-2-aminopropanol during the forward reaction (*41*). The 11 Å separation of the radical and Co^{2+} suggests that the formation of B_{12r} and of the *S*-2-aminopropanol radical occur in separate steps as opposed to a concerted process as has been proposed for the coenzyme B_{12}-dependent ribonucleotide triphosphate reductase (*42*). A Co^{2+}-5′-deoxyadenosyl radical pair in EAL is also indicated by magnetic field and Xe effects on the kinetic parameters (*43*, *44*). These results are therefore consistent with the idea that the 5′-deoxyadenosyl radical is a discrete intermediate in the catalytic cycle of EAL. Models indicate that a simple rotation of the deoxyribosyl moiety around the glycosidic bond (Figure 6) allows the 5′ carbon to shuttle between a bonding position with the Co^{2+} to a location in contact with

the substrate radical. Such rotations have been proposed to move the 5′-deoxyadenosyl radical between Co^{2+} and the substrate in the active site of dioldehydrase (*45*). Such a movement in EAL is supported by recent ^{13}C ENDOR measurements that show that C5′ of 5′-deoxyadenosine lies ~3.4 Å from C-1 of the 2-aminopropanol radical characterized herein (*46*). Pulsed EPR measurements also indicate that there is a pool of three hydrogens (deuterons), consistent with the 5′-methyl group of 5′-deoxyadenosine, which is close to the substrate radical (*47*). The 11 Å separation between the substrate derived radicals and Co^{2+} may represent a natural strategy to minimize turnover inactivation by electron transfer from Co^{2+} to the intermediates as has been documented for lysine 5,6-aminomutase (*48*).

APPENDIX

Analysis of Anisotropies in the Spin−Spin Interaction. The *g*-anisotropy ($g_\perp = 2.26$; $g_\parallel = 2.01$) of the low-spin Co^{2+} in B_{12r} creates the potential for complications in the analysis of the spectra of Co^{2+}/radical pairs (*49*). The dipole−dipole interaction between the radical and Co^{2+} will depend on the position of the radical within the *g*-axis system of B_{12r}, as well as on the orientation of the pair in the external magnetic field (*50*). If the interspin vector is not aligned along a principal axis of the Co^{2+}, the dipole−dipole interaction no longer possesses axial symmetry (*51*). Similarly, spin−orbit coupling, the presence of which is indicated by the anisotropic *g*-tensor, introduces the possibility of anisotropies in the exchange interaction (*52*).

The complexities in the dipole−dipole interaction which arise from *g*-anisotropy can be accommodated within the framework of eq 1. In the most general case, the dipole−dipole interaction and exchange interaction are each described by second rank tensors, **D** and **J**, and each tensor can be decomposed into scalar, vector, and tensor quantities (*34*, *53*). The scalar components of **J** and **D** are combined into *J* (see eq 1). The anisotropic components of **J** and **D** are combined into a conventional zfs tensor wherein the anisotropies are characterized by the axial and rhombic zfs paramters, D and E. Thus, the *J*, D, and E parameters obtained from simulations of the EPR spectra are composites—each parameter includes contributions from dipole−dipole and exchange interactions (*34*):

$$J_o = J_d + J_e$$
$$D = D_d + D_e \qquad \text{(A1)}$$
$$E = E_d + E_e$$

where subscripts d and e denote contributions from dipole−dipole or exchange, respectively.

Anisotropic components of exchange are a result of the spin−orbit coupling within B_{12r} and can have pseudo-dipolar, as well as antisymmetric components, with magnitudes of $(\Delta g/g)^2 J'_e$ and $(\Delta g/g)J'_e$, respectively (*54*). The exchange integrals J'_e are, at present, intractable such that "order-of-magnitude" estimates are generally obtained by replacing J'_e with J_o (*55*). In the active site of EAL, the ~11 Å distance between the radical and Co^{2+} and the modest *g*-anisotropy present in the system are expected to substantially attenuate contributions from anisotropies in the exchange interaction.

Contributions of the dipole−dipole interaction to *J*, D, and E can be evaluated explicitly, and expressions are available for the special case in which the interspin vector is along a principal axis (*34*). A perturbation treatment of pairs having nonparallel axes has also been presented (*56*). The dipole−dipole interaction can be expressed in terms of the interspin distance, *R*, and the position of the interspin vector in the *g*-axis system of the Co^{2+}:

$$\mathbf{D_d} = -\frac{g_2\beta^2}{R^3}\mathbf{D}_{ij} \cdot \mathbf{g_1} \qquad \text{(A2)}$$

where β is the Bohr magneton and $\mathbf{g_1}$ is the *g*-tensor of the low-spin Co^{2+}. Anisotropy in the *g*-tensor of the radical is slight, and this interaction is treated as a scalar quantity, g_2. The dipole−dipole tensor, in its principal axis system, may be represented as follows:

$$\mathbf{D}_{ij} = \begin{pmatrix} 1 & 0 & 0 \\ 0 & 1 & 0 \\ 0 & 0 & -2 \end{pmatrix} \qquad \text{(A3)}$$

If the interspin vector is not aligned with a principal axis of Co^{2+}, an orthogonal transformation, $\mathbf{R} \cdot \mathbf{D}_{ij} \cdot \mathbf{R}^{-1}$, is required to express the dipole−dipole interaction in the *g*-axis system. The axial symmetry of the *g*-tensor of the low-spin Co^{2+} reduces the transformation to a rotation through only one angle, ζ. This transformation is accomplished using the Euler matrix:

$$\mathbf{R} = \begin{pmatrix} \cos\zeta & 0 & -\sin\zeta \\ 0 & 1 & 0 \\ \sin\zeta & 0 & \cos\zeta \end{pmatrix} \qquad \text{(A4)}$$

The final form of $\mathbf{D_d}$ is as follows:

$$\mathbf{D_d} = -\frac{g_2\beta^2}{R^3} \begin{pmatrix} g_\perp(-1 + \cos^2\zeta + \cos 2\zeta) & 0 & -\frac{3}{2}g_\parallel \sin 2\zeta \\ 0 & g_\perp & 0 \\ -\frac{3}{2}g_\perp \sin 2\zeta & 0 & g_\parallel(-2\cos^2\zeta + \sin^2\zeta) \end{pmatrix} \qquad \text{(A5)}$$

Whenever $g_\perp \neq g_\parallel$, $\mathbf{D_d}$ is asymmetric. All off-diagonal terms vanish whenever the interspin vector is along the *z*-axis of the low-spin Co^{2+} ($\zeta = 0°$), and the matrix reduces to

$$\mathbf{D_d}(\zeta = 0°) = -\frac{g_2\beta^2}{R^3}\begin{pmatrix} g_\perp & 0 & 0 \\ 0 & g_\perp & 0 \\ 0 & 0 & -2g_\parallel \end{pmatrix}. \qquad \text{(A6)}$$

The scalar and anisotropic contributions of the dipole−dipole interaction to the spin−spin parameters can be evaluated explicitly. The scalar component of the dipole−dipole interaction, J_d, is equal to 1/3 the trace of $\mathbf{D_d}$:

$$J_d = -\frac{g_2\beta^2}{6R^3}(g_\perp - g_\parallel)(1 + 3\cos 2\zeta). \qquad \text{(A7)}$$

Subtracting J_d from each of the diagonal elements of $\mathbf{D_d}$ (eq 10) gives the traceless tensor, $\mathbf{D'_d}$:

$$\mathbf{D}'_{\mathbf{d}} = -\frac{g_2\beta^2}{R^3}\begin{pmatrix} \frac{1}{6}[-4g_\perp + g_{||} + 3(2g_\perp + g_{||})\cos 2\zeta] & 0 & -\frac{3}{2}g_{||}\sin 2\zeta \\ 0 & \frac{1}{6}[5g_\perp + g_{||} - 3(g_\perp - g_{||})\cos 2\zeta] & 0 \\ -\frac{3}{2}g_\perp \sin 2\zeta & 0 & -\frac{1}{6}(g_\perp + 2g_{||})(1 + 3\cos 2\zeta) \end{pmatrix} \quad \text{(A8)}$$

$\mathbf{D}'_{\mathbf{d}}$ is diagonalized to obtain the principal components of the dipole−dipole interaction, D'_{xx}, D'_{yy}, and D'_{zz}, in terms of the components of the *g*-tensor, the distance, *R*, and the angle, ζ:

$$D'_{xx} = -\frac{g_2\beta^2}{24R^3}\{[-10g_\perp - 2g_{||} + 6(g_\perp - g_{||})\cos 2\zeta] + 3[22g_\perp^2 + 100g_\perp g_{||} + 22g_{||}^2 - 24(g_\perp^2 - g_{||}^2)\cos 2\zeta + 18(g_\perp - g_{||})^2 \cos 4\zeta]^{1/2}\}$$

$$D'_{yy} = -\frac{g_2\beta^2}{6R^3}[5g_\perp + g_{||} - 3(g_\perp - g_{||})\cos 2\zeta] \quad \text{(A9)}$$

$$D'_{zz} = -\frac{g_2\beta^2}{24R^3}[-10g_\perp - 2g_{||} + 6(g_\perp - g_{||})\cos 2\zeta] - 3[22g_\perp^2 + 100g_\perp g_{||} + 22g_{||}^2 - 24(g_\perp^2 - g_{||}^2)\cos 2\zeta + 18(g_\perp - g_{||})^2\cos 4\zeta]^{1/2}$$

The zfs parameters D and E are evaluated, using the principal components of $\mathbf{D}'_{\mathbf{d}}$ (eq A9), and the following relationships (*34*):

$$D = D'_{zz} - 0.5(D'_{xx} + D'_{yy})$$
$$E = 0.5(D'_{xx} - D'_{yy}) \quad \text{(A10)}$$

The rhombicity is defined by:

$$\frac{E}{D} = \frac{a-b}{a+3b}, \quad \text{(A11)}$$

where $a = 10g_\perp + 2g_{||} - 6(g_\perp - g_{||})\cos 2\zeta$ and $b = [22g_\perp^2 + 100g_\perp g_{||} + 22g_{||}^2 - 24(g_\perp^2 - g_{||}^2)\cos 2\zeta + 18(g_\perp - g_{||})^2 \cos 4\zeta]^{1/2}$. As shown in Figure A1, for the extent of *g*-anisotropy exhibited by the low-spin Co^{2+} of B_{12r}, an off-axis alignment of the spins does not impart much rhombicity. The assumption of axial symmetry for the dipole−dipole interaction is valid in the present case.

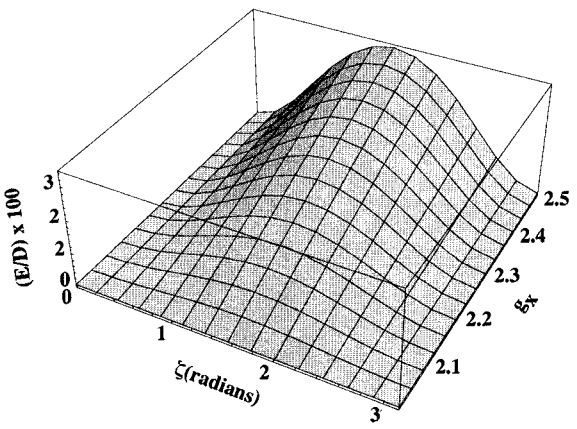

FIGURE A1: Rhombic contribution of dipole−dipole interaction between the radical and Co^{2+} as a function of the orientation (angle) of the interspin vector in the principal axis system of Co^{2+} and of the *g*-anisotropy of Co^{2+}. The angle ζ is the angle between the interspin vector and the g_z-axis of Co^{2+}.

ACKNOWLEDGMENT

The authors are grateful to Dr. B. D. Nageswara Rao for advice on the calculations in the appendix, Mr. Steven O. Mansoorabadi for proofreading of the equations in the appendix, Dr. János Rétey for the sample of ^{15}N-enriched coenzyme B_{12}, and Ms. La Rosa Faust and Dr. Bernard Babior for providing plasmid pKQE4.5.

REFERENCES

1. Babior, B. M. (1982) in *B_{12}* (Dolphin, D., Ed.) John Wiley & Sons, Inc., New York.
2. Babior, B. M. (1988) *BioFactors 1*, 21−26.
3. Bandarian, V., and Reed, G. H. (1999) in *Chemistry and Biochemistry of B_{12}* (Banerjee, R., Ed.) pp 811−833, Wiley-Interscience, New York.
4. Abeles, R. H., and Dolphin, D. H. (1976) *Acc. Chem. Res. 9*, 114−120.
5. Frey, P. A. (1990) *Chem. Rev. 90*, 1343−1357.
6. Stubbe, J., and van der Donk, W. (1998) *Chem. Rev. 98*, 705−762.
7. Hogenkamp, H. P. C. (1999) in *Chemistry and Biochemistry of B_{12}* (Banerjee, R., Ed.) pp 3−8, Wiley-Interscience, New York.
8. Marsh, E. N. G., and Drennan, C. L. (2001) *Current Opinion in Chemical Biology 5*, 499−505.
9. Banerjee, R. (2001) *Biochemistry 40*, 6191−6198.
10. Frey, P. A. (2001) *Annu. Rev. Biochem. 70*, 121−148.
11. Eggerer, H., Stadtman, E. R., Overath, P., and Lynen, F. (1960) *Biochem. Z. 333*, 1−9.
12. Gerfen, G. J., Licht, S., Willems, J. P., Hoffman, B. M., and Stubbe, J. (1996) *J. Am. Chem. Soc. 118*, 8192−8197.
13. Bothe, H., Darley, D. J., Albracht, S. P., Gerfen, G. J., Golding, B. T., and Buckel, W. (1998) *Biochemistry 37*, 4105−4113.
14. Padmakumar, R., and Banerjee, R. (1995) *J. Biol. Chem. 270*, 9295−9300.
15. Babior, B. M., Moss, T. H., Orme-Johnson, W. H., and Beinert, H. (1974) *J. Biol. Chem. 249*, 4537−44.
16. Schepler, K. L., Dunham, W. R., Sands, R. H., Fee, J. A., and Abeles, R. H. (1975) *Biochim. Biophys. Acta 397*, 510−518.
17. Tan, S.-L., Kopczyanski, M. G., Bachovchin, W. W., Orme-Johnson, W. H., and Babior, B. M. (1986) *J. Biol. Chem. 261*, 3483−3485.
18. Ke, S. C., and Warncke, K. (1999) *J. Am. Chem. Soc. 121*, 9922−9927.
19. Boas, J. F., Hicks, P. R., Pilbrow, J. R., and Smith, T. S. (1978) *J. Chem. Soc., Faraday II 74*, 417−430.
20. Buettner, G. R., and Coffman, R. E. (1977) *Biochim. Biophys. Acta 480*, 495−505.
21. Warncke, K., Schmidt, J. C., and Ke, S.-C. (1999) *J. Am. Chem. Soc. 121*, 10522−10528.
22. Faust, L. P., Connor, J. A., Roof, D. M., Hoch, J. A., and Babior, B. M. (1990) *J. Biol. Chem. 265*, 12462−12466.
23. Faust, L. P., and Babior, B. M. (1992) *Arch. Biochem. Biophys. 294*, 50−54.
24. Latwesen, D. G., Poe, M., Leigh, J. S., and Reed, G. H. (1992) *Biochemistry 31*, 4946−4950.
25. Bandarian, V., and Reed, G. H. (1999) *Biochemistry 38*, 12394−12402.
26. Babu, U. M., and Johnston, R. B. (1974) *Biochem. Biophys. Res. Commun. 58*, 460−466.

27. Gerfen, G. J. (1999) in *Chemistry and Biochemistry of B_{12}* (Banerjee, R., Ed.) pp 165−195, Wiley-Interscience, New York.
28. Rieger, P. H. (1982) *J. Magn. Reson. 50*, 485−489.
29. Abend, A., Bandarian, V., Reed, G. H., and Frey, P. A. (2000) *Biochemistry 39*, 6250−6257.
30. Reed, G. H., and Markham, G. D. (1984) *Biol. Magn. Reson. 6*, 73−142.
31. Pake, G. E. (1948) *J. Chem. Phys. 16*, 327−336.
32. Bencini, A., and Gatteschi, D. (1990) *EPR of Exchange Coupled Systems*, Springer-Verlag, New York.
33. Abend, A., Bandarian, V., Nitsche, R., Stupperich, E., Retey, J., and Reed, G. H. (1999) *Arch. Biochem. Biophys. 370*, 138−141.
34. Eaton, G. R., and Eaton, S. S. (1989) *Biol. Magn. Reson. 8*, 650.
35. Wallis, O. C., Bray, R. C., Gutteridge, S., and Hollaway, M. R. (1982) *Eur. J. Biochem. 125*, 299−303.
36. Press, W. H., Flannery, B. P., Teukolsky, S. A., and Vetterling, W. T. (1989) *Numerical Recipes*, Cambridge University Press, New York.
37. Luckhurst, G. R. (1976) in *Spin Labeling: Theory and Applications* (Berliner, L. J., Ed.) pp 592, Academic Press, New York.
38. Taniguchi, H., Fukui, K., Ohnishi, S., Hatano, H., Hasegawa, H., and Maruyama, T. (1968) *J. Phys. Chem. 72*, 1926−1931.
39. Foster, T., and West, P. R. (1973) *Can. J. Chem. 51*, 4009−4017.
40. Ke, S. C., Torrent, M., Museav, D. G., Morokuma, K., and Warncke, K. (1999) *Biochemistry 38*, 12681−12689.
41. Carty, T. J., Babior, B. M., and Abeles, R. H. (1974) *J. Biol. Chem. 249*, 1683−1688.
42. Licht, S. S., Booker, S., and Stubbe, J. (1999) *Biochemistry 38*, 1221−1233.
43. Harkins, T. T., and Grissom, C. B. (1995) *J. Am. Chem. Soc. 117*, 566−567.
44. Anderson, M. A., Xu, Y., and Grissom, C. B. (2001) *J. Am. Chem. Soc. 123*, 6720−6721.
45. Masuda, J., Shibata, N., Morimoto, Y., Toraya, T., and Yasuoka, N. (2000) *Structure Fold Des. 8*, 775−788.
46. LoBrutto, R., Bandarian, V., Magnusson, O. T., Chen, X., Schramm, V. L., and Reed, G. H. (2001) *Biochemistry 40*, 9−14.
47. Warncke, K., and Utada, A. S. (2001) *J. Am. Chem. Soc. 123*, 8564−8572.
48. Tang, K.-H., and Frey, P. A. (2001) *Biochemistry 40*, 5190−5199.
49. Coffman, R. E., and Buettner, G. R. (1979) *J. Phys. Chem. 83*, 2392−2400.
50. Vasavada, K. V., and Nageswara Rao, B. D. (1989) *J. Magn. Reson. 81*, 275−283.
51. Boas, J. F. (1984) in *Copper Proteins and Copper Enzymes* (Lontie, R., Ed.) p 223, CRC Press, Inc., Boca Raton.
52. Bencini, A., and Gatteschi, D. (1990) *EPR of Exchange Coupled Systems*, Springer-Verlog, New York.
53. Abragam, A., and Bleaney, B. (1970) *Electron Paramagnetic Resonance of Transition Ions*, Oxford University Press, London.
54. Moriya, T. (1960) *Phys. Rev. 120*, 91−98.
55. Gatteschi, D., and Bencini, A. (1985) in *Magneto-Structural Correlations in Exchange Coupled Systems* (Willett, R. D., Gatteschi, D., and Kahn, O., Eds.) p 616, D. Reidel Publishing Company, Dordrecht.
56. Carr, S. G., Smith, T. D., and Pilbrow, J. R. (1974) *J. Chem. Soc., Faraday Trans. 2*, 497−511.
57. Hecht, H. G. (1967) *Magnetic Resonance Spectroscopy*, John Wiley & Sons, Inc., New York.

BI0201217